Organic Electronics 52 (2018) 71–78

Contents lists available at ScienceDirect

Organic Electronics

journal homepage: www.elsevier.com/locate/orgel

Optimization, characterization and upscaling of aqueous solar nanoparticle inks for organic photovoltaics using low-cost donor:acceptor blend

Furqan Almyahi[a,b], Thomas R. Andersen[b,*], Nathan Cooling[b], Natalie P. Holmes[b], Adam Fahy[b], Matthew G. Barr[b], David Kilcoyne[c], Warwick Belcher[b], Paul C. Dastoor[b]

[a] Department of Physics, College of Science, University of Basrah, Iraq
[b] Centre for Organic Electronics, University of Newcastle, University Drive, Callaghan, NSW 2308, Australia
[c] Advanced Light Source, Lawrence Berkeley National Laboratory, Berkeley, CA 94720, USA

ARTICLE INFO

Keywords:
Nanoparticles
Organic photovoltaic
Core-shell morphology
Mini-emulsion
Low-cost acceptor

ABSTRACT

We present the optimization and upscaling of water-based nanoparticle inks based on a novel donor-acceptor pair consisting of poly(3-hexylthiophene) (P3HT) and a newly developed indene-C_{60} multiadducts (ICxA) that is comprised of indene-C_{60} monoadduct (ICMA), indene-C_{60} bisadduct (ICBA), and indene-C_{60} trisadduct (ICTA). This material system has been used as a case study to explore the transition from OPV materials optimised for small-scale spin-coating to those optimised for large-scale printing. In particular, we have explored the effects of transitioning from a small-scale BHJ ink formulated from a high-cost acceptor to a large-scale NP ink formulated from a low-cost fullerene mixture. We show that it is possible to use a low-cost acceptor and to formulate the inks at scale with no loss in device performance.

1. Introduction

For almost two decades, organic photovoltaics (OPVs) have been an important area of scientific research, driven primarily by their promise as a low-cost renewable energy source [1,2]. Unlike conventional inorganic solar cells, which require high-purity materials and energy intensive processes, OPVs can in principle be manufactured on a massive scale using roll-to-roll (R2R) coating and printing techniques with substantially lower energy input requirements [3].

However, realising the true potential of OPVs, as expounded in the OPV literature, necessarily requires that the science and technology transitions from small-scale spin-coated devices to larger printed solar modules. Moreover, determining the materials that are best suited to this transition requires new figures of merit that go beyond the traditional benchmarks of device efficiency and lifetime. In particular, material cost becomes a key driver in benchmarking and selection since the key advantage of OPV technology is its low-cost [4].

The cost associated with a particular OPV material system is made up of three main components: (a) intrinsic material cost, (b) scale of material synthesis and (c) material processability. Intrinsic material cost is associated with the complexity required to synthesise the organic electronic materials. For example, the fewer the number of synthetic steps and the less work up required to purify the final material, the lower the cost. Likewise, the greater the scale of material synthesis the lower the cost of the final product. Finally, the more processable the materials are with regards to the final fabrication process the lower is the cost to manufacture the final OPV module.

1.1. Intrinsic material cost

Recent commercial models for roll-to-roll (R2R) manufacturing of OPVs show that the cost-of-materials (COM) dominates the total module costs [5]. Consequently, despite years of work on high efficiency materials [6,7], our work has shown that the workhorse poly(3-hexylthiophene) (P3HT): phenyl-C61-butyric acid methyl ester (PCBM) blend system currently offers the most realistic pathway to large scale OPV production due to its low intrinsic material cost [4].

We have recently reported the development of a new low-cost fullerene (ICxA) that can be used as a direct replacement for the commonly used electron acceptor PCBM in OPVs [8]. ICxA is a novel indene-adducted fullerene acceptor mixture that, when blended with P3HT, can deliver device efficiencies comparable to those obtained for P3HT:PCBM blends but at an even lower intrinsic material cost due to its simpler synthetic and purification requirements [8].

1.2. Scale of materials

As well as the intrinsic material cost there are two other aspects of

* Corresponding author.
E-mail address: thomas.andersen@newcastle.edu.au (T.R. Andersen).

http://dx.doi.org/10.1016/j.orgel.2017.10.008
Received 11 August 2017; Received in revised form 18 September 2017; Accepted 7 October 2017
Available online 12 October 2017

the preparation of commercial scale inks that need to be considered. Firstly, the scale of materials synthesis directly impacts the COM of the final manufactured module, with lower costs realised as scale increases [9,10]. As well as lower net raw material input costs, the costs associated with the overall synthesis and purification are reduced since alternative processing pathways are possible when dealing with materials at scale [11]. Secondly, the cost of formulating the synthesised materials into inks is also reduced when dealing with materials at large scale since again new processing pathways can be applied.

1.3. Material processability

In general, the techniques applied for R2R manufacturing, such as slot-die coating, screen printing and flexographic printing, require wet processable materials which, in the case of OPV materials, are typically obtained through the addition of heavily chlorinated solvents (chloroform and mono-, bi-, tri- chloro adducted benzenes) [12,13]. These solvents are highly hazardous to both human and environmental health and attempts to eliminate chlorinated solvents from the manufacturing process have been underway for many years [14]. Importantly, current international regulations heavily restrict the use of volatile organic solvents and consequently the cost of implementing these solvent systems for large-scale manufacturing is prohibitive [15,16].

Initial approaches used less harmful solvent systems such as alcohols, ketones or other aromatic hydrocarbons such as ortho-xylene, which, while better than chloroform or chlorobenzene, are not without risk [17,18].

The general consensus within the printing industry and associated regulatory bodies is that, from a health perspective, aqueous-based ink systems are the most preferable coating and printing solution [19] but other green solvents (such as alcohols) are of interest as they lower the risk albeit without eliminating it; offering the prospect of highly processible OPV material systems that could be applied to a wide variety of printing processes without the need for costly volatile solvent handling infrastructure.

The transition from organic solvent to water-based inks has been attempted by three different pathways: (a) side-chain modification with non-ionic alcohol or glycol chains, (b) ionic side-chain modification such as ammonium, sulfonic acid or carboxylic acid and (c) the development of nanoparticle (NP) dispersions where hydrophobic material blends are dispersed in water or alcohols. There are two developed pathways for this approach firstly there is a surfactant stabilized nanoparticle approach, this laboratory has for many years continuously developed the surfactant-based NP-OPV approach since it can readily be applied to a wide range of existing material systems without molecular modification by processing them into water-dispersible nanoparticles [20–23].

The second approach is to use surfactant-free nanoparticles which have shown great potential in literature with more than 4% efficiency reported for a P3HT:ICBA nanoparticle system [24]. The major drawback of this procedure is that the prepared NP solutions are very unstable with major aggregation occurring within hours [25], which is undesirable if applying these NP in an industrial setting. This instability is not observed for surfactant stabilized NP ink, which is why we have chosen to employ this ink type as the base of our study. In contrast to these NP approaches, creating aqueous materials via side-chain modification necessarily requires a complete material redesign and processing redevelopment encompassing film formation, phase separation and crystallinity [26].

In this paper we explore the relative role that these three factors play in determining the viability of OPV for commercial application. In particular, we study the implementation of an inherently low cost acceptor material (ICxA) in NP OPV devices based on both laboratory scale and large scale materials synthesis.

2. Experimental

2.1. Materials and equipment for NP inks

To synthesise the NP inks, we used poly(3-hexylthiophene) (P3HT) (M_n 23 kDa, PDI 1.42) and a low-cost mixed fullerene acceptor blend consisting of 51% ICBA, 36% ICMA and 13% ICTA called ICxA made in house as previously reported [8]. In addition, sodium dodecyl sulphate (SDS) with 98% purity was obtained from Sigma-Aldrich, as a surfactant. PEDOT:PSS Clevios HTL Solar was purchased from Heraeus. Mini-emulsions were prepared for small and large volume nanoparticles using a Hielscher ultrasound booster horn UIP400S (400 W, 24 kHz) with a sonotrode of 3 mm diameter or UIP1000hdT (1000 W, 20 kHz) with a sonotrode of 22 mm diameter, respectively. The obtained nanoparticles dispersions were purified by ultrafiltration against water through a PES membrane with a cut-off at 10 kDa MWCO. Small batches were purified via centrifugal ultrafiltration using centrifugal ultrafiltration tubes (Vivaproducts), whereas large batches were dialyzed using a Vivaflow 200 crossflow cassette (Sartorius) and a peristaltic pump.

2.2. Preparation of NP inks

An aqueous dispersion of small and large-batches of nanoparticles P3HT:ICxA were synthesised by a modified mini-emulsion method [27,28]. In this work small and large volume NP P3HT:ICxA inks were synthesised individually using similar preparation conditions excluding ultrasound treatments and ultrafiltration processes (A photographic overview of large batch ASNP preparation can be found in Fig. 1). As can be seen in Table 1, the organic phase was prepared by dissolving the (30–53.6 mg mL^{-1}) P3HT:ICxA blend (1:0.8 ratio) in chloroform with stirring at 35 °C and 500 rpm for 60 min. The aqueous phases were prepared by dissolving (11.8 mg mL^{-1}) SDS in Milli-Q water with stirring at 25 °C and 500 rpm for 30 min. The P3HT:ICxA solution was injected drop by drop into the SDS solution with continuous stirring at room temperature and 1200 rpm to produce the macro-emulsions. The formed macro-emulsions were then ultrasonically treated to form a mini-emulsion; small batches were treated for 2 min at 60% amplitude and a power of 30–34 W and large batches for 10 min at 100% amplitude and a power of 450–500 W. During ultrasonication of the large batches we had to use a beaker with large height to width ratio in order to accommodate the increased emulsion volume that occurs as gas gets trapped in the SDS network. Chloroform was removed from the mini-emulsions for small batches by stirring at 1200 rpm for 4 h at 60 °C to produce aqueous nanoparticle P3HT:ICxA dispersions. In addition, for large batch synthesis it was necessary to reduce the temperature to 55 °C for the first hour to avoid spillage and to arrange a layer of insulation (cottonwool and aluminium foil) around the beaker during chloroform evaporation. These dispersions were purified to eliminate the excess SDS and finally concentrated to 60 mg mL^{-1}. The small volume NP dispersions (2.5 mL) were purified using dialysis and centrifugal ultrafiltration at 3550 rpm for 7 min eliminating 2 mL of SDS containing Milli-Q water, refilled with 2 mL Milli-Q water (this elimination and addition was repeated 5 times) and the ink was finally concentrated to 0.5 mL. Large-volume dispersions (500 mL) were purified and concentrated using the viva 200 flow cell cartridge ultrafiltration system with pressure across the filter of 1.2 bar pressure ending up with a volume of 100 mL of NP ink.

2.3. Dynamic light scattering (DLS)

Dynamic light scattering measurements were conducted on the ASNP inks with large and small-volumes to analyse particle sizes. Samples with 0.03 mg mL^{-1} were prepared by diluting the 5 μL of ASNPs (60 mg mL^{-1}) with 10000 μL of water. Measurements were made on a Zetasizer Nano ZS (Malvern Instruments) at room

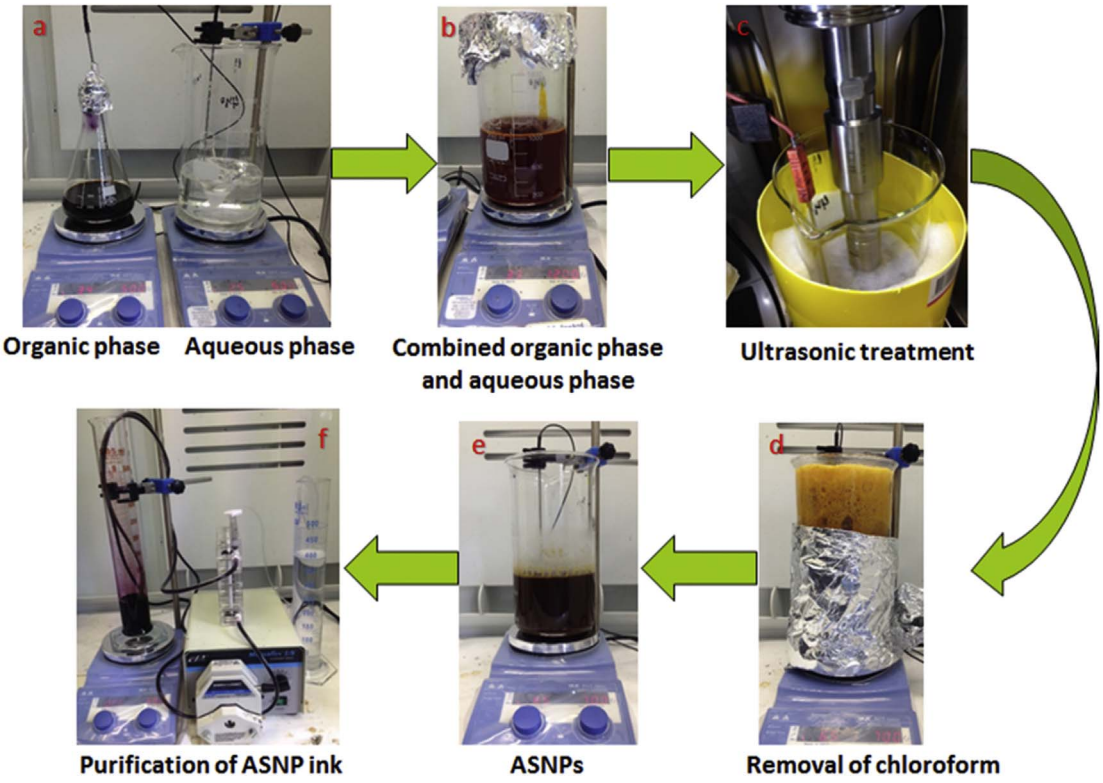

Fig. 1. Photographic presentation of each step for large scale NP preparation. (a) Image of the two pure phases, organic phase (left) and aqueous SDS solution (right). (b) Macro-emulsion formation by combining the two phases. (c) Mini-emulsion formation by treating the macro-emulsion with ultrasound. (d) Nanoparticle formation by removal of chloroform. (e) The non-purified ASNP ink has formed after removal of chloroform and turned from orange to deep purple. (f) Purification of ASNP inks by cross-flow ultrafiltration. (For interpretation of the references to colour in this figure legend, the reader is referred to the web version of this article.)

temperature using disposable cuvettes.

2.4. Optical microscopy

For the optical microscopy investigations, nanoparticle films were spin-coated at 2000 rpm onto pre-cleaned glass slides and probed by using the optical microscope attachment on an Asylum Research Cypher atomic force microscope with 10× magnification.

2.5. Atomic force microscopy (AFM)

An Asylum Research Cypher atomic force microscope (AFM) operated in AC mode was used to probe the nanoparticle films. Film samples for AFM were spin-coated on quartz glass substrates at 2000 rpm for 1 min.

2.6. Device fabrication and photocurrent density-voltage testing

Although spin-coating is not an industrially applicable process, it has been used here to produce OPV devices to benchmark the performance of both small batch and large batch NP dispersions. Unfortunately, this comparison is not possible utilizing a R2R slot-die coating head, which has a dead volume of 50 mL, when the small batches of NP ink are typically 0.5 mL. NP-OPV devices were fabricated in normal geometry with the structure ITO/PEDOT:PSS/NP P3HT:ICxA/Ca/Al. Patterned ITO glass substrates were cleaned using detergent solution, water, acetone and IPA with sonication for 5 min each. Using spin-coating (5000 rpm, 1 min) PEDOT:PSS films (35 ± 5 nm) were formed on ITO glass substrates, and dried at 150 °C for 20 min in fume-hood. After cooling to room temperature, 35 μL of P3HT:ICxA nanoparticle inks were spin-coated on the PEDOT:PSS coated ITO glass substrates to form nanoparticle layers with a thicknesses of 105 ± 7 nm, nanoparticle films were dried at 110 °C for 5 min. These substrates were directly transferred to nitrogen glovebox and dried again at 110 °C for 5 min. The thermal evaporation of calcium (Ca) and aluminium (Al) on active layers were performed in vacuum (2×10^{-6} Torr), and thicknesses of Ca and Al electrodes were monitored by quartz crystal monitor to be 30 nm and 100 nm, respectively. Using a Newport class A solar simulator with an AM 1.5 spectrum filter the photocurrent density-voltage (J-V) curves were obtained for NP-OPV devices with areas of 3.8 mm^2 as dried and annealed at 140 °C for 4 min.

Table 1
Preparation parameters for small and large-volume NP inks.

Ink Scale	Aqueous Phase		Organic Phase		NP Inks		
	Wt (mg)	Vol (mL)	Wt (mg)	Vol (mL)	Wt (mg)	Vol (mL)	Conc. (mg mL^{-1})
53.6 mg mL^{-1} (small)	33	2.8	30	0.56	30	0.50	60
30.0 mg mL^{-1} (small)	33	2.8	30	1.0	30	0.50	60
Large	6600	560	6000	112	6000	100	60
Large STXM sample	100	280	3000	112	3000	100	30

2.7. NEXAFS and STXM

Pristine film samples were prepared for near-edge X-ray absorption fine structure (NEXAFS) measurements by spin coating films of P3HT and ICxA from solvent onto PEDOT:PSS coated glass and floating off onto 300 mesh copper grids. Phase separation of the three ICxA components (ICMA, ICBA and ICTA) was noted on spin coating, which was attributed to solubility differences between the components, hence the X-ray beam was defocused to collect a reference NEXAFS spectrum representative of the average ICxA film composition. NP samples were prepared for scanning transmission X-ray microscopy (STXM) by spin coating 2.5 μL of NP dispersion onto low stress silicon nitride (Si_3N_4) windows with silicon dioxide coating (window dimensions 0.25 × 0.25 mm^2, window thickness 15 nm, frame 5 × 5 mm^2) (purchased from Norcada, Canada) at 3000 rpm, 1 min, low acceleration of 112 rpm s^{-1}. Nanoparticles prepared for STXM morphological investigation had a reduced concentration of surfactant in the miniemulsion aqueous phase (0.36 mg mL^{-1}) with the aim of achieving both larger particles and a broad distribution in particle sizes for imaging. Non-annealed (or 'as cast') samples were air dried. NEXAFS and STXM measurements were performed on beamline 5.3.2.2 at the Advanced Light Source. NEXAFS spectra were used to identify key absorption energies for P3HT and ICxA, following this the NP samples were rastered with respect to the X-ray beam to generate absorption maps. SVD (singular value decomposition) fitting was then performed to generate composition maps for P3HT and ICxA, with further detail of the method of measurement reported elsewhere [29].

3. Results and discussion

3.1. Optimization of P3HT:ICxA NP OPVs based on laboratory scale ink formulation

Small scale synthesis of P3HT:PCBM and P3HT:ICBA NPs have been reported previously and the resultant inks have been optimised for OPV devices [22,30]. These optimised conditions (organic material = 53.6 mg mL^{-1} in chloroform, SDS = 11.8 mg mL^{-1} in Milli-Q water) have been shown to be general for a range of material systems [23,31,32] and as such were the logical starting point for the initial P3HT:ICxA formulation. However, films prepared from these NP inks were of poor quality as seen in Fig. 2a, where a number of larger aggregates are clearly visible. Whilst the solubility of ICBA (> 90 mg mL^{-1} in chloroform) is comparable to that of PCBM (> 90 mg mL^{-1} in chloroform) [33], the solubility of the mono-adducted fullerene component (ICMA) in ICxA is much lower (measured as ~ 5 mg mL^{-1} in our laboratory). Therefore, we hypothesised that the poor film quality was a consequence of undissolved ICMA acting as nucleation sites for aggregation during drying. This hypothesis was tested by preparing a new series of inks with a concentration of the organic phase of 30 mg mL^{-1}, corresponding to ICMA = 4.8 mg mL^{-1}. Films prepared from the resulting inks revealed a significantly enhanced film quality with no larger aggregates present as seen in Fig. 2b. AFM images of film prepared with inks from both concentrations can be found in Fig. S1 in supplementary information, as seen from these there doesn't appear to be any difference between the films on a microscopic level only on a macroscopic level. Despite the difference in film quality, the overall film composition appears to be similar as illustrated by the absorption curves, in Fig. 2c, with only minor differences observed both as a function of concentration and annealing. Devices prepared from 53.6 mg mL^{-1} to 30 mg mL^{-1} inks had quite different photovoltaic characteristics (Fig. 2d) with the higher concentration as dried devices exhibiting a power conversion efficiency (PCE) of 0.51% while the lower concentration as dried devices had a PCE of 0.28%. Upon annealing, the PCE of the higher (53.6 mg mL^{-1}) concentration devices decreased significantly from 0.51% to 0.13% due to decreases of 56 and 38% in V_{OC} and J_{SC}, respectively. By contrast, the lower (30 mg mL^{-1}) concentration devices exhibited a threefold increase in PCE from 0.28% to 0.88%; mainly due to an increase in J_{SC} of approximately 150% but also a 23% increase in V_{OC}. The external quantum efficiency (EQE) curves in Fig. 2e confirm the J_{sc} behaviour observed in the J-V data, with the as dried 30 mg mL^{-1} device being the lowest followed by the annealed 53.6 mg mL^{-1} device, the annealed 30 mg mL^{-1} device exhibits the highest EQE and as dried 53.6 mg mL^{-1} device is in between.

3.2. Optimization of P3HT:ICxA NP OPVs based on large scale ink formulation

In order to probe the effect of the scale of material synthesis on device performance, we developed an upscaled process for ink fabrication; increasing the ink volume from 0.5 mL per batch to 100 mL batches. Upscaling the ink preparation required a change from a centrifuge based ultrafiltration purification method to a crossflow based technique whereby a dialysis filter is used to concentrate the inks via excess water and SDS migrating through the filter driven by the pressure difference between the two sides. From the optical microscopy images in Fig. 3a and b, it can be seen that while annealing causes some minor aggregation on the film surface there is significantly less aggregation than was observed for 53.6 mg mL^{-1} small scale formulation NP films. An AFM image has also been obtained for a film prepared from ink from a large ASNP batch (see Fig. S1), which appears very similar to the AFM images obtained from the small batches. Minor differences were observed in the absorption spectra of as spun and annealed NP films, which can be ascribed to minor inhomogeneities rather than a higher ICxA concentration in the as spun NP film. OPV devices were prepared from the upscaled NP batch and the photovoltaic characteristics are shown in Fig. 3d and the table in Fig. 3. Upon annealing the PCE of these devices increases from 0.33% to 0.87%, primarily due to increases in V_{OC} and J_{SC} with only a minor increase in FF from 35% to 39%. The increase in J_{SC} correlates well with the EQE spectra (Fig. 3e) where the EQE increases from a maximum value of approximately 15% to approximately 30% upon annealing.

To further investigate the upscaling process the particle sizes for the three ASNP inks were determined by DLS. The volumetric size distribution of ASNP inks from large and small batches (53.6 and 30 mg mL^{-1}) can be found in Fig. 4. As seen there are only minor differences in particle size; particles from the 30 mg mL^{-1} batch are slightly smaller (32 ± 7 nm) than large-batch particles (34 ± 9 nm) which in turn is smaller than 53.6 mg mL^{-1} (38 ± 9 nm). These sizes showed us that is it possible to make a 200 fold upscaling with only minor if any effect on the sizes of the obtained particles.

3.3. Internal phase separation investigation

A determining factor for the efficiencies obtained with NP devices is the internal morphology of the nanoparticle i.e. phase separation, domain sizes, material crystallinity etc. Scanning transmission X-ray microscopy (STXM) was used to probe the structure and composition of the as spun P3HT:ICxA NPs. Near edge X-ray absorption fine structure (NEXAFS) spectra of the pristine materials are shown in Fig. 5a, and were used to determine the orthogonal photon energies of 284.4 eV and 287.4 eV used for the mass plots of ICxA and P3HT, respectively. STXM measurements of the as cast NP films provide insight into the internal P3HT:ICxA NP morphology, as evident from the composition plots of P3HT and ICxA shown in Fig. 5c and d, respectively. The nanoparticles have a clear core shell structure with a core consisting primarily of ICxA and P3HT being present dominantly in shell. These distributions are similar to those obtained by Ulum et al. for as-spun P3HT:ICBA NPs [30]; indicating that the presence of a mixed acceptor doesn't alter the typical core-shell structure seen for NP materials.

Fig. 6a shows the fractional P3HT composition as a function of normalised radial distance for a set of 19 analysed P3HT:ICxA nanoparticles of varying sizes (approximately 100–200 nm). The radial

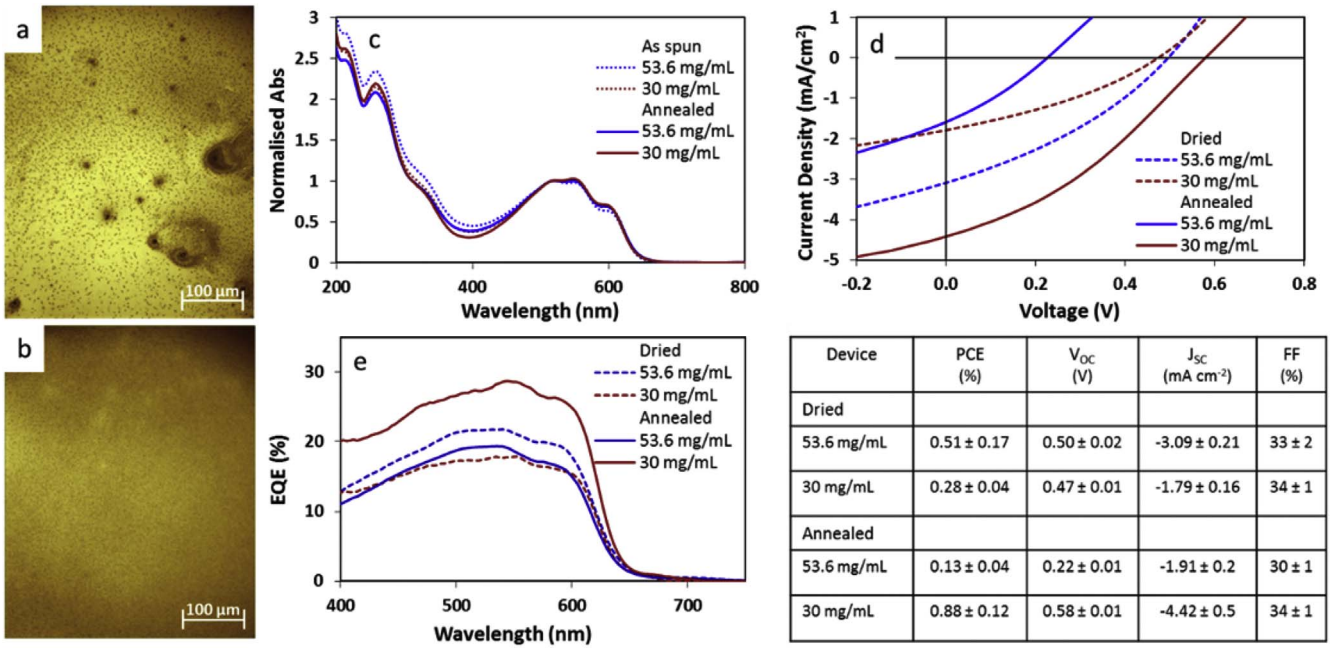

Device	PCE (%)	V_{OC} (V)	J_{SC} (mA cm^{-2})	FF (%)
Dried				
53.6 mg/mL	0.51 ± 0.17	0.50 ± 0.02	-3.09 ± 0.21	33 ± 2
30 mg/mL	0.28 ± 0.04	0.47 ± 0.01	-1.79 ± 0.16	34 ± 1
Annealed				
53.6 mg/mL	0.13 ± 0.04	0.22 ± 0.01	-1.91 ± 0.2	30 ± 1
30 mg/mL	0.88 ± 0.12	0.58 ± 0.01	-4.42 ± 0.5	34 ± 1

Fig. 2. (a) and (b) presents optical microscopy image of an annealed film prepared from 53.6 mg mL^{-1} to 30 mg mL^{-1} nanoparticles, respectively (scale bars are 100 µm). (c) Normalised absorption curves of nanoparticle batches prepared with a concentration of 53.6 mg mL^{-1} and 30 mg mL^{-1} both as spun and annealed at 140 °C for 4 min (d) J-V curves of hero devices as prepared with nanoparticles prepared with a concentration of 53.6 mg mL^{-1} and 30 mg mL^{-1} both dried (110 °C) and annealed at 140 °C for 4 min. (e) External quantum efficiencies of hero devices of 53.6 mg mL^{-1} and 30 mg mL^{-1} both as dried and annealed. Table with averaged photovoltaic characteristics and standard deviation based on 12 devices.

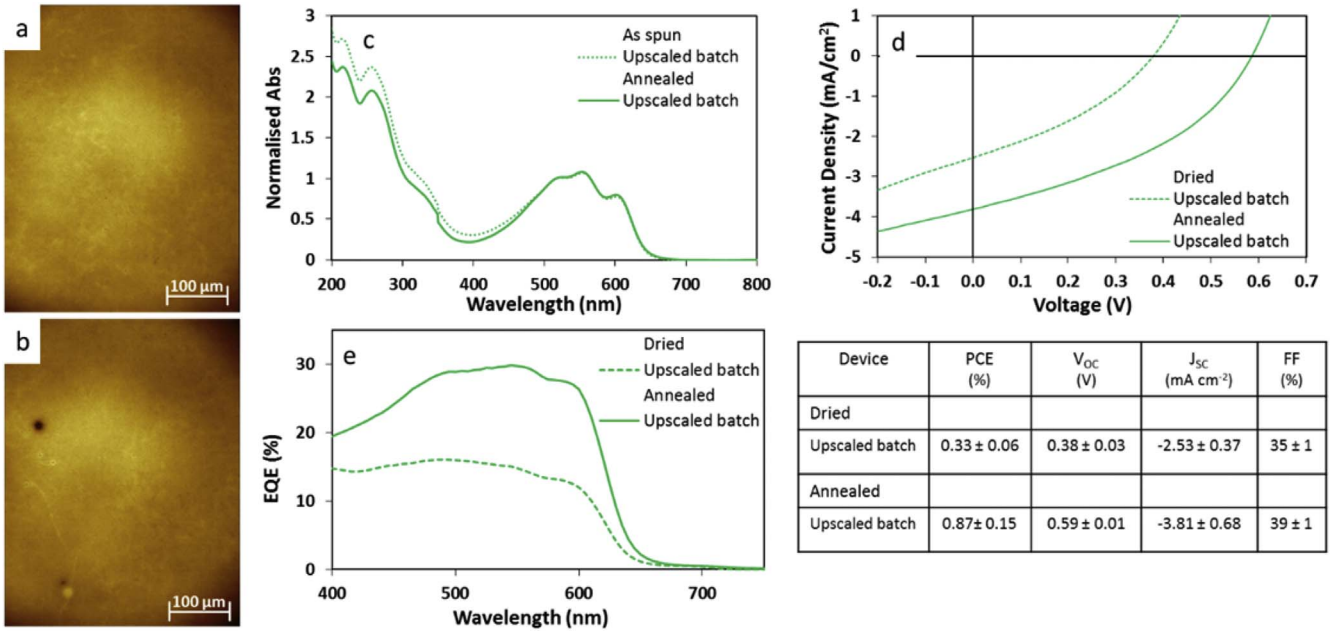

Device	PCE (%)	V_{OC} (V)	J_{SC} (mA cm^{-2})	FF (%)
Dried				
Upscaled batch	0.33 ± 0.06	0.38 ± 0.03	-2.53 ± 0.37	35 ± 1
Annealed				
Upscaled batch	0.87± 0.15	0.59 ± 0.01	-3.81 ± 0.68	39 ± 1

Fig. 3. (a) and (b) presents optical microscopy images of a dried and annealed film, respectively. (c) Absorption spectra of NP films prepared from the upscaled batch both as annealed and as spun. (d) J-V curves of hero devices as prepared with the upscaled nanoparticles batch both as dried (110 °C) and annealed at 140 °C for 4 min. (e) External quantum efficiencies of hero devices both as dried and annealed. Table with averaged photovoltaic characteristics and standard deviation based on 12 devices.

compositional profiles were obtained across arcs of the compositional map that were clear of neighbouring particles and then integrated to give an average composition as a function of distance from the centre of the particle [34]. Normalisation of the radial distance was obtained by setting the radial distance of maximum P3HT concentration to unity for each particle and scaling the radial component of the compositional profile accordingly. Each normalised compositional profile was interpolated to a common set of radial intervals and the mean composition as a function of the normalised radial distance was subsequently calculated (solid red line in Fig. 6a). The mean compositional profile confirms a core-shell morphology, with fractional P3HT shell and core compositions of 0.48 ± 0.05 and 0.22 ± 0.07 respectively. The results show that the particle core and shell domain compositions are enhanced in ICxA concentration relative to the original P3HT:ICxA solution ratio (1:0.8) used for the NP synthesis. Fig. 6b shows that, by comparison, the fractional P3HT core and shell domain compositions for P3HT:PCBM (1:1 [21]) and P3HT:ICBA (1:0.8 [30]) more closely represent the initial P3HT:fullerene solution ratios used for the NP synthesis. Moreover from the data in Fig. 6b it is evident that the material composition difference of donor and acceptor between core and

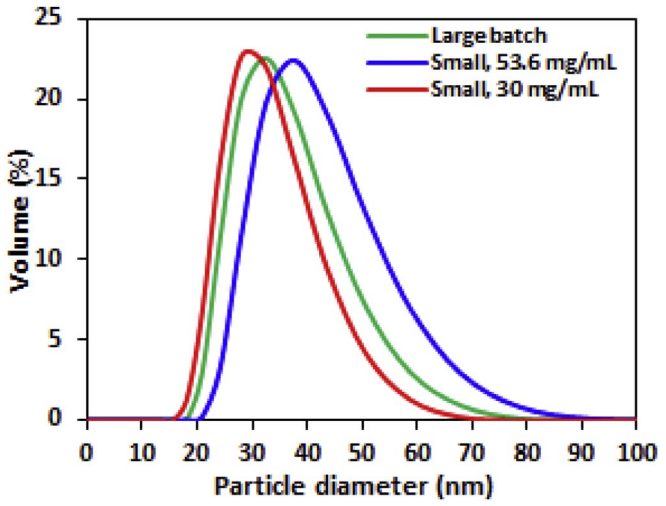

Fig. 4. Volumetric size distribution for the ANSP inks, small 30 mg mL^{-1} is the solid red line, small 53.6 mg mL^{-1} is the blue line and the large batch is the green line. (For interpretation of the references to colour in this figure legend, the reader is referred to the web version of this article.)

shell, with a difference of 28 and 26% points, are much closer for nanoparticles based on P3HT:ICBA and P3HT:ICxA, respectively, than for particles based on P3HT:PCBM with 44% points.

3.4. Comparing material cost, processability and formulation scale

Fig. 7 illustrates the three factors that govern the COM in large scale manufactured OPV devices. For each factor (cost, processability and scale) we argue that in general OPV technology needs to transition to intrinsically lower cost materials that can be processed from acceptable solvents using inks formulated at scale. In this paper, we have explored this argument for a particular case study based on transitioning from the P3HT:PCBM BHJ system to the P3HT:ICxA NP OPV system.

Previous work has shown that, despite the fact that ICxA is a mixture of fullerenes rather than a single fullerene component (enabling its low intrinsic cost), OPV devices made from ICxA perform as well as those from PCBM [8]. As such, the P3HT:ICxA blend offers one pathway to the development of an intrinsically low cost material system; allowing us to move along the Cost axis from PCBM to ICxA in Fig. 7, as the cost of 1 g of ICxA is 17 AUD [8] whereas 1 g of PCBM is 180 AUD, when purchasing on a 50 g scale from Solenne, without any appreciable loss in device performance.

By contrast, even though research groups have spent the better part of a decade developing a wide variety of ink and material systems for NP OPV devices, their efficiency is still reduced (~50%) in comparison to their bulk heterojunction counterparts [30,35,36]. Until recently it was speculated that the presence of the applied surfactant was the cause for the reduced efficiency. It has, however, been shown that the actual cause is poor dissociation of excitons generated in the polymer-rich domain [37,38]. This issue has been linked to non-optimal phase-separation within the nanoparticle, which for P3HT:PCBM nanoparticles comprises a core-shell structure with an acceptor-rich core and donor-rich shell [23,39]. One of the few material systems tested for nanoparticular OPVs without exhibiting a core-shell phase-separation is P3HT:ICBA which, in contrast to P3HT:PCBM, develops highly mixed phases upon annealing with the resulting devices for P3HT:ICBA doubled in efficiency compared to P3HT:PCBM [22,30]. For the P3HT:ICxA NP OPV system, we also see a reduction in the efficiency of small-scale NP devices (PCE ~ 0.9%) compared to the corresponding BHJ devices (PCE ~ 2.8% [8]) suggesting that charge generation remains an issue in the P3HT:ICxA NP system. Indeed, this is further supported by the observation that NP:BHJ efficiency ratio is similar in both cases, being 0.37 and 0.32 for P3HT:ICBA and P3HT:ICxA, respectively. However, recent modelling of the levelised cost of electricity for OPVs suggests that even modest improvements (~1%) in device efficiency would place these devices within the commercially viable range for certain applications [4].

By comparison, the results from the small batch optimised ink preparation and the upscaled batch correlate very well with device efficiencies of 0.88 and 0.87%, respectively. In addition, the film formation properties have been maintained despite a 200-fold increase in the ink formulation volume. As such, we have demonstrated that moving along the Scale axis in Fig. 7 from SML to LGE scale of ink

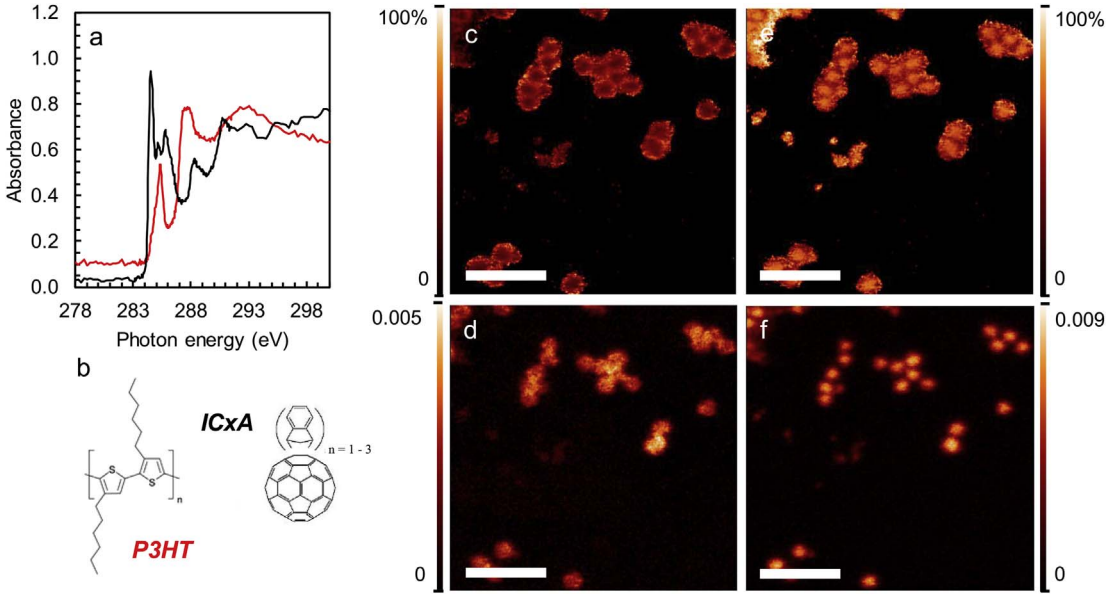

Fig. 5. (a) Near edge X-ray absorption fine structure (NEXAFS) spectra of P3HT (red) and ICxA (black). (b) Chemical structure of P3HT (red) and ICxA (black). (b) STXM fractional composition maps of 1:1 P3HT:ICxA nanoparticles as cast (no thermal treatment) showing the concentration of (c) P3HT and (e) ICxA, with (d, f) corresponding STXM mass plots. All scale bars are 1 μm. The colour contrast is scaled such that light colours correspond to higher component concentrations. Minima and maxima for the colour scale bar in (c) and (e) are black = 0 and white = 100%. For (d) and (f) the colour scale bars indicate concentration of component in mg cm^{-2}. (For interpretation of the references to colour in this figure legend, the reader is referred to the web version of this article.)

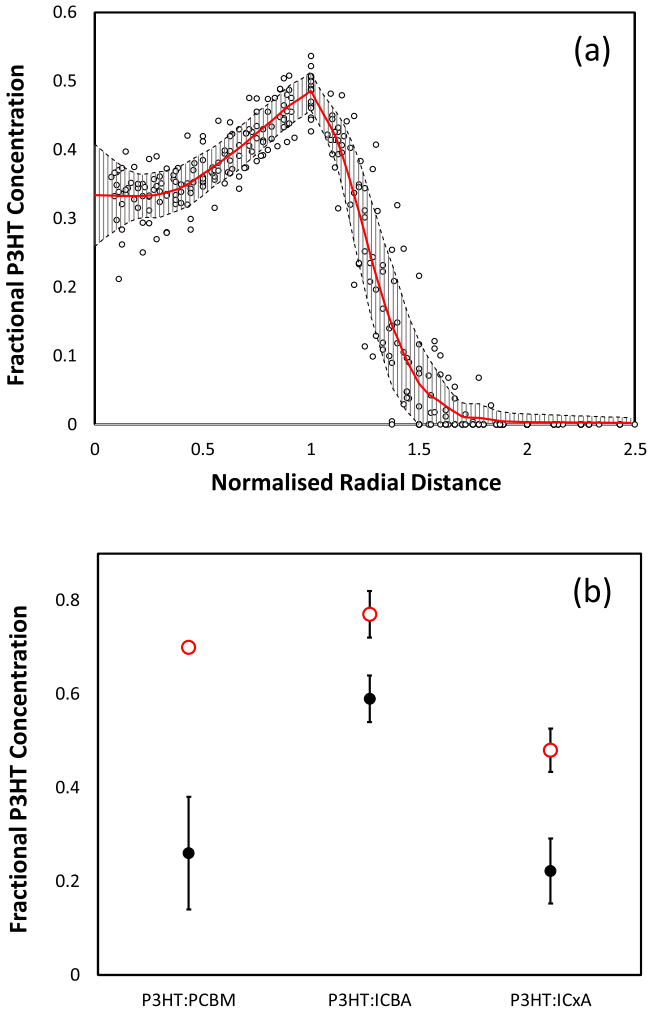

Fig. 6. (a) Plot of fractional P3HT composition as a function of normalised radial distance for the set of analysed P3HT:ICxA nanoparticles (open black circles). The solid red line denotes the mean composition. The dashed black lines denote the size of the standard deviation in the mean composition. The hashed area denotes the region lying within the 95% confidence limit of the mean value. (b) Mean fractional P3HT concentration for the nanoparticle shell (open red circles) and core (closed black circles) domains for P3HT:PCBM [21], P3HT:ICBA [30] and P3HT:ICxA as-spun nanoparticles. The error bars are obtained from the standard deviation of the radial analysis. (For interpretation of the references to colour in this figure legend, the reader is referred to the web version of this article.)

formulation does not detrimentally impact on the performance of the NP devices and that device efficiency is maintained for large scale ink formulations.

4. Conclusion

In this manuscript we present the preparation of water based nanoparticular inks from a novel donor-acceptor system based on blends of P3HT and ICxA; an intrinsically low-cost mixed fullerene acceptor. The as-spun nanoparticles had a core-shell internal structure with an ICxA-rich core and a P3HT concentration that is enhanced in the shell relative to the core; consistent with observations for other polymer:fullerene nanoparticle morphologies. This material system has been used as a case study to explore the transition from OPV materials optimised for small-scale spin-coating to those optimised for large-scale printing. In particular, we have explored the effects of transitioning from a small scale BHJ ink formulated from a high-cost acceptor to a large-scale NP ink formulated from a low-cost fullerene mixture. We show that it is possible to use a low-cost acceptor and to formulate the

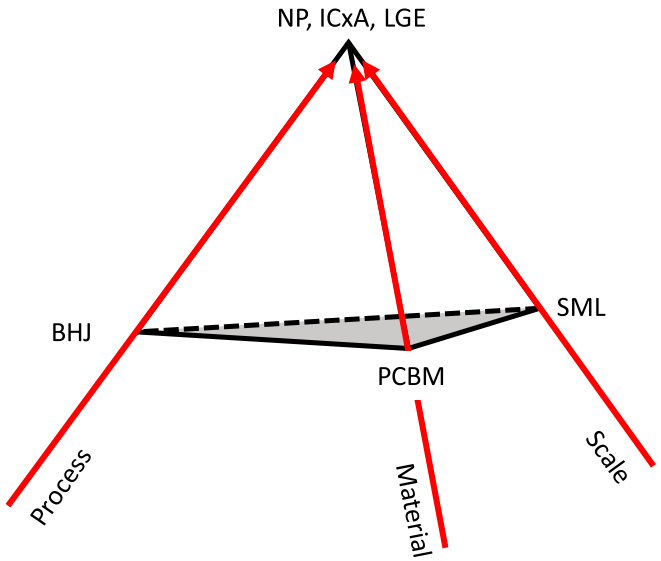

Fig. 7. Schematic diagram illustrating the three main factors contributing to the COM in OPV devices: (i) material processability (Process axis), (ii) intrinsic material cost (Material axis) and (iii) scale of materials (Scale axis). In this case study, the process transition is from BHJ to NP, the intrinsic materials cost transition is from PCBM to ICxA and the scale of materials transition is from laboratory (SML) scale formulation to large (LGE) scale formulation.

inks at scale with no loss in device performance. In addition, we have shown that it is possible to upscale the ink preparation by a factor of 200 whilst maintaining device efficiency with an average PCE of 0.87% achieved for the large-scale ink formulation.

Acknowledgement

Furqan Almyahi gratefully acknowledge the Office of the Prime Minister of Iraq through the Higher Committee for Education Development (HCED) for funding support. The work was performed in part at the Materials node of the Australian National Fabrication Facility, a company established under the National Collaborative Research Infrastructure Strategy to provide nano- and microfabrication facilities for Australia's researchers. The ALS is supported by the Director, Office of Science, Office of Basic Energy Sciences, of the U.S. Department of Energy under Contract No. DE-AC02-05CH11231.

Appendix A. Supplementary data

Supplementary data related to this article can be found at http://dx.doi.org/10.1016/j.orgel.2017.10.008.

References

[1] S.B. Darling, F. You, The case for organic photovoltaics, RSC Adv. 3 (2013) 17633–17648.
[2] P.G.V. Sampaio, M.O.A. González, Photovoltaic solar energy: conceptual framework, Renew. Sustain. Energy Rev. 74 (2017) 590–601.
[3] N. Espinosa, R. García-Valverde, A. Urbina, F.C. Krebs, A life cycle analysis of polymer solar cell modules prepared using roll-to-roll methods under ambient conditions, Sol. Energy Mater. Sol. Cells 95 (2011) 1293–1302.
[4] C.J. Mulligan, C. Bilen, X. Zhou, W.J. Belcher, P.C. Dastoor, Levelised cost of electricity for organic photovoltaics, Sol. Energy Mater. Sol. Cells 133 (2015) 26–31.
[5] C.J. Mulligan, M. Wilson, G. Bryant, B. Vaughan, X. Zhou, W.J. Belcher, P.C. Dastoor, A projection of commercial-scale organic photovoltaic module costs, Sol. Energy Mater. Sol. Cells 120 (2014) 9–17.
[6] S.Q. Zhang, L. Ye, J.H. Hou, Breaking the 10% efficiency barrier in organic photovoltaics: morphology and device optimization of well-known PBDTTT polymers, Adv. Energy Mater. 6 (2016) 1502529.
[7] J. Huang, X. Zhang, D. Zheng, K. Yan, C.-Z. Li, J. Yu, Boosting organic photovoltaic performance over 11% efficiency with photoconductive fullerene interfacial modifier, Sol. RRL 1 (2017) 1600008.

[8] N.A. Cooling, E.F. Barnes, F. Almyahi, K. Feron, M.F. Al-Mudhaffer, A. Al-Ahmad, B. Vaughan, T.R. Andersen, M.J. Griffith, A.S. Hart, A.G. Lyons, W.J. Belcher, P.C. Dastoor, A low-cost mixed fullerene acceptor blend for printed electronics, J. Mater. Chem. A 4 (2016) 10274–10281.
[9] R. Po, J. Roncali, Beyond efficiency: scalability of molecular donor materials for organic photovoltaics, J. Mater. Chem. C 4 (2016) 3677–3685.
[10] A. Gambhir, P. Sandwell, J. Nelson, The future costs of OPV – a bottom-up model of material and manufacturing costs with uncertainty analysis, Sol. Energy Mater. Sol. Cells 156 (2016) 49–58.
[11] T.P. Osedach, T.L. Andrew, V. Bulovic, Effect of synthetic accessibility on the commercial viability of organic photovoltaics, Energy Environ. Sci. 6 (2013) 711–718.
[12] F.C. Krebs, Fabrication and processing of polymer solar cells: a review of printing and coating techniques, Sol. Energy Mater. Sol. Cells 93 (2009) 394–412.
[13] R.R. Søndergaard, M. Hösel, F.C. Krebs, Roll-to-Roll fabrication of large area functional organic materials, J. Polym. Sci. Part B Polym. Phys. 51 (2013) 16–34.
[14] R.K. Henderson, C. Jimenez-Gonzalez, D.J.C. Constable, S.R. Alston, G.G.A. Inglis, G. Fisher, J. Sherwood, S.P. Binks, A.D. Curzons, Expanding GSK's solvent selection guide - embedding sustainability into solvent selection starting at medicinal chemistry, Green Chem. 13 (2011) 854–862.
[15] A.M. Ruder, Potential health effects of occupational chlorinated solvent exposure, Ann. N. Y. Acad. Sci. 1076 (2006) 207–227.
[16] E.M. Ward, P.A. Schulte, K. Straif, N.B. Hopf, J.C. Caldwell, T. Carreon, D.M. DeMarini, B.A. Fowler, B.D. Goldstein, K. Hemminki, C.J. Hines, K.H. Pursiainen, E. Kuempel, J. Lewtas, R.M. Lunn, E. Lynge, D.M. McElvenny, H. Muhle, T. Nakajima, L.W. Robertson, N. Rothman, A.M. Ruder, M.K. Schubauer-Berigan, J. Siemiatycki, D. Silverman, M.T. Smith, T. Sorahan, K. Steenland, R.G. Stevens, P. Vineis, S.H. Zahm, L. Zeise, V.J. Cogliano, Research recommendations for selected IARC-classified agents, Environ. Health Perspect. 118 (2010) 1355–1362.
[17] O. Synooka, K.R. Eberhardt, H. Hoppe, Chlorine-free processed high performance organic solar cells, RSC Adv. 4 (2014) 16681–16685.
[18] C.-C. Chueh, K. Yao, H.-L. Yip, C.-Y. Chang, Y.-X. Xu, K.-S. Chen, C.-Z. Li, P. Liu, F. Huang, Y. Chen, W.-C. Chen, A.K.Y. Jen, Non-halogenated solvents for environmentally friendly processing of high-performance bulk-heterojunction polymer solar cells, Energy Environ. Sci. 6 (2013) 3241–3248.
[19] Environmental Action for the Printing Industry, Dept. of Environment and Conservation, Sydney South, N.S.W, 2006.
[20] B. Vaughan, A. Stapleton, E. Sesa, N.P. Holmes, X.J. Zhou, P.C. Dastoor, W.J. Belcher, Engineering vertical morphology with nanoparticulate organic photovoltaic devices, Org. Electron. 32 (2016) 250–257.
[21] N.P. Holmes, N. Nicolaidis, K. Feron, M. Barr, K.B. Burke, M. Al-Mudhaffer, P. Sista, A.L.D. Kilcoyne, M.C. Stefan, X. Zhou, P.C. Dastoor, W.J. Belcher, Probing the origin of photocurrent in nanoparticulate organic photovoltaics, Sol. Energy Mater. Sol. Cells 140 (2015) 412–421.
[22] S. Ulum, N. Holmes, D. Darwis, K. Burke, A.L. David Kilcoyne, X. Zhou, W. Belcher, P. Dastoor, Determining the structural motif of P3HT: PCBM nanoparticulate organic photovoltaic devices, Sol. Energy Mater. Sol. Cells 110 (2013) 43–48.
[23] N.P. Holmes, M. Marks, P. Kumar, R. Kroon, M.G. Barr, N. Nicolaidis, K. Feron, A. Pivrikas, A. Fahy, A.D.d.Z. Mendaza, A.L.D. Kilcoyne, C. Müller, X. Zhou, M.R. Andersson, P.C. Dastoor, W.J. Belcher, Nano-pathways: bridging the divide between water-processable nanoparticulate and bulk heterojunction organic photovoltaics, Nano Energy 19 (2016) 495–510.
[24] S. Gärtner, M. Christmann, S. Sankaran, H. Röhm, E.-M. Prinz, F. Penth, A. Pütz, A.E. Türeli, B. Penth, B. Baumstümmler, A. Colsmann, Eco-Friendly fabrication of 4% efficient organic solar cells from surfactant-free P3HT: ICBA nanoparticle dispersions, Adv. Mater. 26 (2014) 6653–6657.
[25] D. Darwis, N. Holmes, D. Elkington, A.L.D. Kilcoyne, G. Bryant, X.J. Zhou, P. Dastoor, W. Belcher, Surfactant-free nanoparticulate organic photovoltaics, Sol. Energy Mater. Sol. Cells 121 (2014) 99–107.
[26] D.A. Rider, B.J. Worfolk, K.D. Harris, A. Lalany, K. Shahbazi, M.D. Fleischauer, M.J. Brett, J.M. Buriak, Stable inverted polymer/fullerene solar cells using a cationic polythiophene modified PEDOT: PSS cathodic interface, Adv. Funct. Mater. 20 (2010) 2404–2415.
[27] K. Landfester, R. Montenegro, U. Scherf, R. Guntner, U. Asawapirom, S. Patil, D. Neher, T. Kietzke, Semiconducting polymer nanospheres in aqueous dispersion prepared by a miniemulsion process, Adv. Mater. 14 (2002) 651–655.
[28] T. Kietzke, D. Neher, K. Landfester, R. Montenegro, R. Guntner, U. Scherf, Novel approaches to polymer blends based on polymer nanoparticles, Nat. Mater. 2 (2003) 408–412.
[29] N.P. Holmes, B. Vaughan, E.L. Williams, R. Kroon, M.R. Anderrson, A.L.D. Kilcoyne, P. Sonar, X. Zhou, P.C. Dastoor, W.J. Belcher, Diketopyrrolopyrrole-based polymer:fullerene nanoparticle films with thermally stable morphology for organic photovoltaic applications, MRS Commun. 7 (2017) 67–73.
[30] S. Ulum, N. Holmes, M. Barr, A.L.D. Kilcoyne, B.B. Gong, X. Zhou, W. Belcher, P. Dastoor, The role of miscibility in polymer:fullerene nanoparticulate organic photovoltaic devices, Nano Energy 2 (2013) 897–905.
[31] A. Stapleton, B. Vaughan, B. Xue, E. Sesa, K. Burke, X. Zhou, G. Bryant, O. Werzer, A. Nelson, A.L. David Kilcoyne, L. Thomsen, E. Wanless, W. Belcher, P. Dastoor, A multilayered approach to polyfluorene water-based organic photovoltaics, Sol. Energy Mater. Sol. Cells 102 (2012) 114–124.
[32] N.P. Holmes, S. Ulum, P. Sista, K.B. Burke, M.G. Wilson, M.C. Stefan, X. Zhou, P.C. Dastoor, W.J. Belcher, The effect of polymer molecular weight on P3HT: PCBM nanoparticulate organic photovoltaic device performance, Sol. Energy Mater. Sol. Cells 128 (2014) 369–377.
[33] Y. He, H.-Y. Chen, J. Hou, Y. Li, Indene−C60 bisadduct: a new acceptor for high-performance polymer solar cells, J. Am. Chem. Soc. 132 (2010) 1377–1382.
[34] K.B. Burke, A.J. Stapleton, B. Vaughan, X. Zhou, A.L.D. Kilcoyne, W.J. Belcher, P.C. Dastoor, Scanning transmission x-ray microscopy of polymer nanoparticles: probing morphology on sub-10 nm length scales, Nanotechnology 22 (2011) 265710.
[35] M. Bag, T.S. Gehan, L.A. Renna, D.D. Algaier, P.M. Lahti, D. Venkataraman, Fabrication conditions for efficient organic photovoltaic cells from aqueous dispersions of nanoparticles, RSC Adv. 4 (2014) 45325–45331.
[36] L. D'Olieslaeger, G. Pirotte, I. Cardinaletti, J. D'Haen, J. Manca, D. Vanderzande, W. Maes, A. Ethirajan, Eco-friendly fabrication of PBDTTPD: PC71BM solar cells reaching a PCE of 3.8% using water-based nanoparticle dispersions, Org. Electron. 42 (2017) 42–46.
[37] M. Bag, T.S. Gehan, D.D. Algaier, F. Liu, G. Nagarjuna, P.M. Lahti, T.P. Russell, D. Venkataraman, Efficient charge transport in assemblies of surfactant-stabilized semiconducting nanoparticles, Adv. Mater. 25 (2013) 6411–6415.
[38] X. Han, M. Bag, T.S. Gehan, D. Venkataraman, D. Maroudas, Analysis of charge transport and device performance in organic photovoltaic devices with active layers of self-assembled nanospheres, J. Phys. Chem. C 119 (2015) 25826–25839.
[39] H.F. Dam, N.P. Holmes, T.R. Andersen, T.T. Larsen-Olsen, M. Barr, A.L.D. Kilcoyne, X. Zhou, P.C. Dastoor, F.C. Krebs, W.J. Belcher, The effect of mesomorphology upon the performance of nanoparticulate organic photovoltaic devices, Sol. Energy Mater. Sol. Cells 138 (2015) 102–108.